Dark-soliton dynamics and snake instability in superfluid Fermi gases trapped by an anisotropic harmonic potential

Wen Wen and Changqing Zhao
Department of Mathematics and Physics, Hohai University, Changzhou Campus, Changzhou 213022, China

Xiaodong Ma
College of Physics and Electronic Engineering, Xinjiang Normal University, Urumchi 830054, China

(Received 22 September 2013; published 11 December 2013)

We present an investigation of generation, dynamics, and stability of dark solitons in anisotropic Fermi gases for a range of particle numbers and trap aspect ratios within the framework of the order-parameter equation. We calculate the periods of dark solitons oscillating in a trap and find good agreement with the results based on the Bogoliubov–de Gennes equations. By studying the stability of initially off-center dark solitons under various tight transverse confinements in the unitarity limit, we not only give the criterion of dynamical stability, but also find that the soliton and a hybrid of solitons and vortex rings can be characterized by different oscillation periods. The stability criterion is not fulfilled by the parameters of the recent experiment of Yefsah *et al*. [Nature (London) **499**, 426 (2013)]. Therefore, instead of a very slow oscillation as observed experimentally, we find that the created dark soliton undergoes a transverse snake instability with a collapse into vortex rings, which propagate in solitonlike manner with a nearly 2 times larger period.

DOI: 10.1103/PhysRevA.88.063621 PACS number(s): 03.75.Ss, 03.75.Lm

I. INTRODUCTION

Dark solitons, namely, localized density dips with a phase jump across their density minimum, are the most fundamental nonlinear excitations in nonlinear dispersive media. They appear in many areas of science, such as water waves, nonlinear optics, biophysics, and plasma and particle physics [1], and more recently in Bose-Einstein condensates [2–4]. Since the first observation of the crossover from a Bardeen-Cooper-Schrieffer (BCS) superfluid to a Bose-Einstein condensation (BEC) in ultracold fermionic atomic gases [5–9], understanding the formation, dynamics, and stability of solitons in a strongly interacting fermionic system has attracted great attention [10,11] and explored theoretically [12–19].

Based on the BCS mean-field theory [20], the existence and properties of black solitons in the BCS-BEC crossover were demonstrated [12] by the real solutions of the Bogoliubov–de Gennes (BdG) equations. The more general case of the complex solutions corresponding to gray solitons was also considered [13,16]. Subsequently, the periodic dynamics of dark solitons in a harmonic trap [14,15] and two-soliton collisions [16] were studied by numerically solving the time-dependent BdG equations. It was predicted that the oscillation period of a soliton in a harmonic trap increases as one moves from the BEC to BCS regimes [14,15]. From the computational side, calculating solutions to both the time-independent and time-dependent BdG equations is numerically intensive, since they require self-consistent calculations of single-particle states whose number increases linearly with the number of particles. For this reason, these investigations have essentially been restricted to Fermi gases confined in a box [12,13] or one-dimensional (1D) trapping potential [15,16] and for small numbers of atoms, which is essentially quasi-1D. However, this is not particularly relevant to current experimental settings.

In the very recent MIT experiment performed by Yefsah *et al*., with a fermionic superfluid of ^{6}Li near a Feshbach resonance the long-lived solitons were observed [11]. These authors created dark solitons by phase imprinting in the cigar-shaped superfluid. Instead of *in situ* imaging solitons at the Feshbach resonance, the visualization of solitons relied on the time-of-flight method. It was obtained after releasing the superfluid cloud from its trap and letting it expand with the rapid ramp to the weakly interacting BEC regime. Then the oscillation period of dark solitons in the unitary regime was measured, which was 10 times larger than that predicted by the BCS mean-field theory [14,15]. Note that Yefsah *et al*. essentially prepared the superfluid Fermi gases containing about 2×10^5 atom pairs and confined them in an external anisotropic harmonic trap, which is not satisfied by the quasi-1D condition. Hence this is of great interest in the generation, dynamics, and stability of dark solitons in a genuinely three-dimensional (3D) superfluid Fermi gas.

Different from previous investigations by the extended BdG equations [12–16], our theoretical investigations are based on the time-dependent order-parameter equation [21,22]. The order-parameter equation can only describe superfluidity features macroscopically, but its mathematical framework is simple, involving only a single function of the coordinate, i.e., the superfluid density. Thus we encounter no limitation in the number of particles and external potentials, and the analysis is simple and clear. Our calculation is carried out for a wide range of atom numbers and trap aspect ratios. We not only present the oscillation periods of dark solitons in the trapped Fermi gases containing a small number of atoms, but we also find that as the number of atoms is increased by 2 orders, the period of stable solitons increases 8%. By examining the effects of transverse confinement on the stability of initially off-center solitons through their phase profiles, we give the criterion of dynamical stability. Finally, we find that the dark soliton created in the MIT experiment is subject to snake instability,

splitting into two vortex rings and eventually reducing to one vortex ring, which performs a solitonlike oscillatory motion.

This paper is organized as follows: After a brief description of the order-parameter equation and the numerical method in Sec. II, the dynamics of dark solitons in the quasi-1D regime is studied in Sec. III, and the soliton periods along the BCS-BEC crossover are compared with those obtained from the BdG equations. In Sec. IV, the snake instability of a dark soliton in the unitary limit is studied and the dynamic stability criterion is given. The results of our calculation on the dark-soliton dynamics in the parameters of the MIT experiment are presented in Sec. V. Finally, a conclusion is given in Sec. VI.

II. MODEL AND METHOD

We consider an ultracold Fermi gas at zero temperature in which fermionic atoms have two spin states with equal number. In a ground state all atoms are paired and in the superfluid state, which can be described by the following time-dependent order-parameter (or macroscopic wave function) equation [21–29]:

$$i\hbar\frac{\partial\Psi_s}{\partial t}=\left[-\frac{\hbar^2\nabla^2}{2M}+V_s(\mathbf{r})+\mu_s(n_s)\right]\Psi_s, \tag{1}$$

where Ψ_s is the order parameter of fermionic atomic pairs in the superfluid state. This complex quantity can be specified by its magnitude and its phase, $\Psi_s=|\Psi_s|e^{i\Phi_s}$. The pair density in the superfluid state equals $n_s=|\Psi_s|^2$, which should be discriminated from the condensate density. So the normalized condition is given by $\int d\mathbf{r}|\Psi_s|^2=N$, where N is the total atomic pair number of the superfluid Fermi gas, also equal to the number in each spin state. The superfluid velocity is given in terms of the order-parameter phase by the relation $\mathbf{v}_s=\hbar\nabla\Phi_s/M$ [2,22], where we have used the mass of atom pair M (i.e., $M=2m$, with m being atomic mass).

Defining a dimensionless interaction parameter $\eta\equiv 1/(k_Fa_s)$, where k_F is the Fermi wave number and a_s is s-wave scattering length, one can distinguish several different superfluid regimes: a BCS regime ($\eta\leqslant -1$), a BEC regime ($\eta\geqslant 1$), and a BCS-BEC crossover regime ($-1<\eta<1$). A special case $\eta=0$ is called the unitarity limit where the scattering length is infinity. The BCS-BEC crossover regime is a strongly interacting regime, while BCS ($\eta\ll -1$) and BEC ($\eta\gg 1$) limits are actually weakly interacting. In general, the expression for the equation of state $\mu_s(n_s)=2\mu(n)$, with $n=2n_s$ being the atomic superfluid density, is very complicated, but it can be fitted by the analytical formula based on the Monte Carlo data [30] and approximated by the polytropic approximation [31–33]:

$$\mu_s(n_s)=2\mu^0(n_s/n^0)^\gamma, \tag{2a}$$

$$\gamma=\gamma(\eta)=\frac{n}{\mu}\frac{\partial\mu}{\partial n}=\frac{\frac{2}{3}\sigma(\eta)-\frac{2\eta}{5}\sigma'(\eta)+\frac{(\eta)^2}{15}\sigma''(\eta)}{\sigma(\eta)-\frac{\eta}{5}\sigma'(\eta)}, \tag{2b}$$

where μ^0 and n^0 are reference chemical potential and particle number density, respectively [33]. Usually we take the reference particle number density $n^0=(2mE_F)^{3/2}/(6\pi^2\hbar^3)$ to be the per spin density of the noninteracting Fermi gas at the trapping center, and the reference chemical is thus $\mu^0=E_F[\sigma(\eta)-\eta\sigma'(\eta)/5]$, proportional to the Fermi energy $E_F=(\hbar k_F)^2/(2m)$. The order-parameter equation incorporated with the equation of state allows one to investigate the smooth crossover from the BEC limit to the BCS regime [34] in a unified way.

It is noticed that in the unitarity limit ($\eta=0,\gamma=2/3$), the order-parameter equation is exactly equivalent to one derived by Salasnich *et al.* from an extended Thomas-Fermi density functional theory [21]. In the BEC limit ($\eta\gg 1,\gamma=1$), the order-parameter equation coincides exactly with an equation derived by Pieri and Strinati based on BdG equations [35]. Very recently, Forbes and Sharma [36] presented a comparison between the Fermi superfluid dynamics in the unitary limit using the local density functional theory [37] and the order-parameter equation, and very similar results were found.

It has been demonstrated that the order-parameter equation is very reliable to capture ground-state properties [27,32] and low-energy collective dynamics [27,33] in the BCS-BEC crossover. Furthermore, the results given by the order-parameter equation in the BEC side of the crossover are found to be in good agreement with the zero-temperature BdG equations [38,39]. However, the order-parameter equation cannot completely capture dynamical properties in the BCS regime ($\eta<0$), because dynamical behaviors can easily result in pair breaking due to a very small gap energy [40], while the order-parameter equation ignores single-particle excitation.

We consider a cylindrically symmetric harmonic trap

$$V_s(\mathbf{r})=\tfrac{1}{2}M\omega_z^2(\lambda^2r^2+z^2), \tag{3}$$

where (r,z) are cylindrical coordinates with $r=\sqrt{x^2+y^2}$. The aspect ratio (anisotropy) of the trap is defined by $\lambda=\omega_\perp/\omega_z$, with the trapping frequencies $\omega_\perp$ and ω_z. So the Fermi energy for the fermions trapped by a 3D harmonic potential is given by $E_F=\hbar(6N\omega_\perp^2\omega_z)^{1/3}$. The axial trapping frequency is $\omega_z=2\pi\times 10.66$ Hz in the MIT experiment [11], and the transversal frequency $\omega_\perp=\lambda\omega_z$ is determined by fixing the axial frequency and different aspect ratios. We choose the total number of atom pairs in a wide range, $N=2\times 10^5\sim 2\times 10^2$. In the following, the length is in units of $a_z\equiv\sqrt{\hbar/(M\omega_z)}=8.89$ μm and time is in units of axial trapping period $T_z\equiv 2\pi/\omega_z=93.8$ ms [11]. Two-dimensional density profiles are presented by normalized cross-sectional densities in the $y=0$ plane, i.e., $n_s(x,z)=\frac{a_z^3}{2\sqrt{2}N}|\Psi_s(x,y=0,z)|^2$.

Recently we have presented the dark-soliton solutions of quasi-1D order-parameter equations by the multiple-scale method in the small-amplitude limit [18]. Later, bell solitons along the BCS-BEC crossover as exact soliton solutions of the order-parameter equation in arbitrary amplitudes were found analytically [19]. In the MIT experiment, dark solitons in Fermi gases were created by means of the phase imprinting technique [11], which originally was proposed to generate vortices and solitons in weakly interacting atomic BECs [41], and experimentally implemented [42,43]. The main idea of this technique is described as shining an off-resonance laser on a condensate in order to create phase steps between its different parts. Instead of exposing the analytic 1D soliton solution [19] to 3D, we simulate the phase imprinting method to generate initial solitons in anisotropic Fermi gases along the BCS-BEC crossover.

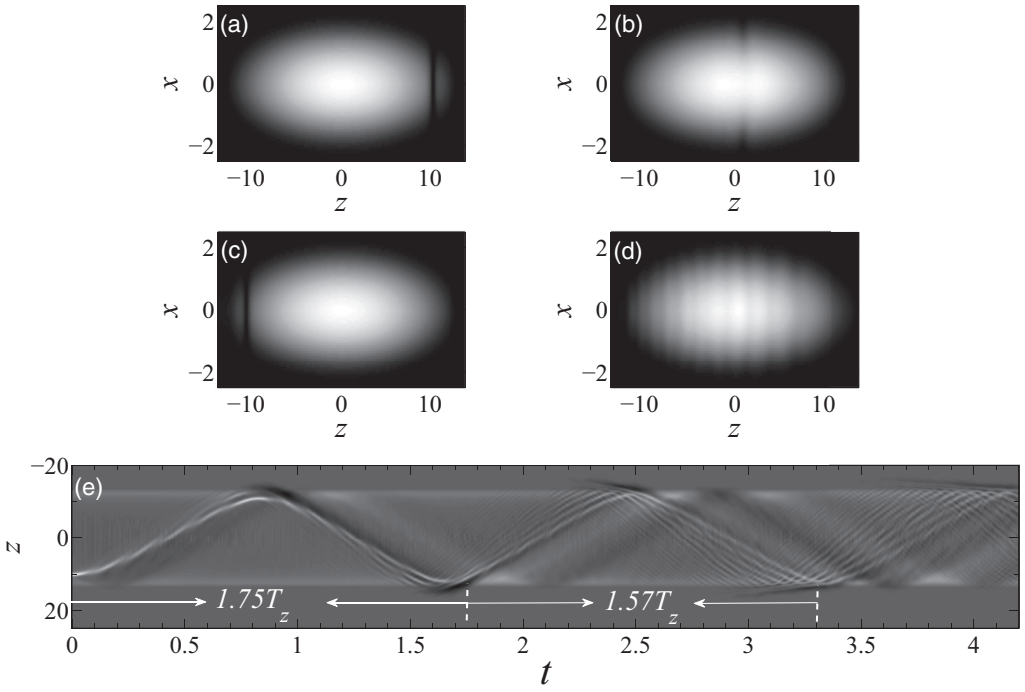

FIG. 1. Dark soliton dynamics in anisotropic superfluid Fermi gases in the unitarity limit, with total atom pairs $N = 2 \times 10^2$ and aspect ratio $\lambda = 6.5$. Plane (a) shows the initial density profiles of dark soliton generated at the axial position $z_0 = 3R_z/4$, with R_z being the axial half length. Planes (b), (c), and (d) are snapshots of dark-soliton dynamics at times $t = 0.4$, $t = 0.8$, and $t = 3.6$, respectively. Light and dark regions indicate high and low densities. Plane (e) is the spatiotemporal contour plot of the renormalized density (the ground-state density minus the actual axial density) at the $r = 0$ plane. The dark soliton oscillates in the trap with the first period of $1.75T_z$ and the reduced second of $1.57T_z$.

We solve the order-parameter equation by discretizing with the split-step Crank-Nicolson algorithm [44]. The initial dark soliton is created by employing imaginary time propagation subject to an enforced axially symmetric π phase step, and then its dynamics is calculated by using real-time propagation.

III. THE SOLITON PERIODS ACROSS THE BCS-BEC CROSSOVER

The beginning of our calculation is to apply the parameters $N = 2 \times 10^2$ and $\lambda = 6.5$ for the superfluid Fermi gas in the unitarity limit ($\eta = 0$). By imposing a π phase step at the axial position $z_0 = 3R_z/4$, with R_z being the axial half length, the density profile evolves into that of an axially symmetric dark soliton shown in Fig. 1(a). This off-center dark soliton under harmonic confinement is expected to oscillate back and forth along the trap as a quasiparticle [45–47]. Figures 1(b)–1(d) depict the density profiles of the dark soliton at different evolution times. As shown in Fig. 1(b), the initial black soliton moves towards the trap center at $t = 0.4$ from the right side, in which it becomes a shallower gray soliton due to the higher density near the center the faster it gets. For the time scale of the axial trapping period $t = 0.8$ in Fig. 1(c), the soliton is prone to be unstable, emitting radiation in the form of sound waves. After long-lived oscillations accompanied by the sound waves at $t = 3.6$, the dark soliton completely decays into a train of sound waves [see Fig. 1(d)].

In order to monitor the soliton trajectory, we present the spatiotemporal evolution by the renormalized density (the time-independent ground-state density without a soliton minus the actual density) along a cross section at $r = 0$ in Fig. 1(e), where the soliton and sound waves are indicated by the light regions. Figure 1(e) provides a clearer indication of dynamical instability in the form of sound radiation and gives the first period of the dark soliton oscillating in the trap to be $T_s = 1.75T_z$. It is shown that the dissipation of energy by the sound waves from the soliton is associated with an increase of amplitude of oscillation (antidamping) and the soliton becomes shallower; as a result, it accelerates with the second oscillation period of $1.57T_z$.

Such dynamical decay of a moving soliton via the emission of sound waves can be accounted for by two instability mechanisms in the framework of the order-parameter equation: (i) axial background inhomogeneity due to the trapping potential [46,48–50] and (ii) the effects of transverse degree of freedom coupled with the axial degree by the atomic interaction [46,51–53].

The relevant size of solitons in the crossover from the BEC limit up to the unitary limit can be characterized by the healing length $\xi = \hbar/\sqrt{2M\mu_s}$, with local chemical potential $\mu_s(\mathbf{r})$ depending on the spatially inhomogeneous density $n_s(\mathbf{r})$. The local chemical potential is determined by the ground-state solution of the order-parameter equation Eq. (1), that is, $\mu_s(\mathbf{r}) + V_s(\mathbf{r}) = \mu_G$. By using the normalized condition, one can obtain the bulk chemical potential μ_G [33]. In the presence of the harmonic trap, the axial size of the superfluid $R_z = \sqrt{2\mu_G/M\omega_z^2}$ is set by the trapping frequency. For the case of Fig. 1, we find that $R_z/\xi = 2\sqrt{\mu_s\mu_G}/\hbar\omega_z = 63$, which

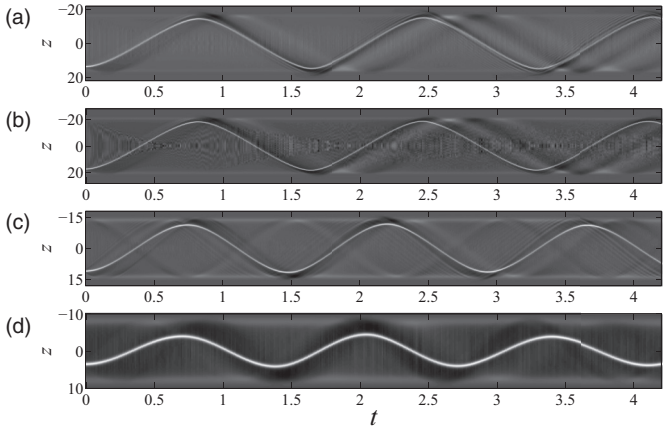

FIG. 2. The spatiotemporal contour plots of dark-soliton dynamics in superfluid Fermi gases containing $N = 2 \times 10^2$ atomic pairs. (a) Corresponds to $\eta = 0$ (the unitarity limit) with aspect ratio $\lambda = 15$, and (b) for $\eta = 0$ with $\lambda = 30$; and (c) and (d) are for $\eta = 1.0$ (BEC side) and $\eta = 6.0$ (BEC limit), respectively, both with $\lambda = 30$.

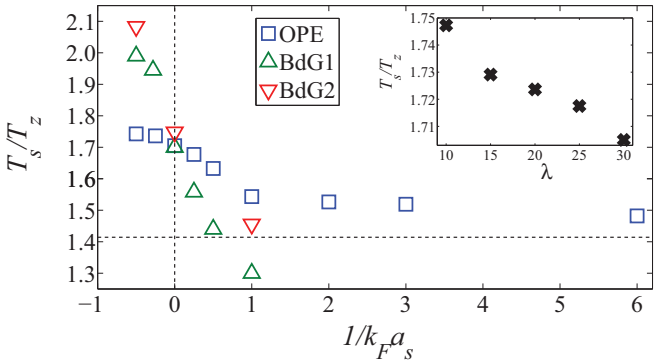

FIG. 3. (Color online) Periods of dark solitons in the quasi-1D regime along the BCS-BEC crossover. Our results (□), based on the order-parameter equation, are compared with those from the the BdG equations by Scott *et al.* (△) [14] and Liao and Brand (▽) [15]. The horizontal dashed line indicates the well-known period $\sqrt{2}T_z$ for atomic BECs. The inset shows the periods of the soliton oscillating in the unitarity limit as a function of the aspect ratio.

means that the change in the axial background is very weak over the size of the soliton.

On the other hand, the characteristic size of the soliton is the order of the healing length, thus the corresponding (axial) kinetic energy is the order of μ_s. The dimensionality parameter defined by $\alpha = \mu_s/\hbar\omega_\perp = 3.22$ implies that the kinetic energy is larger than the transverse energy $\hbar\omega_\perp$, and the atomic interaction can induce transfer of axial energy to the transversal degrees of freedom. Therefore, we conclude that the dominant decay mechanism is due to the coupling to transverse modes.

To suppress the dynamical instability, we perform a stronger transverse confinement of their motion, that is, $\lambda = 15$ ($\alpha = 2.44$ correspondingly). Therefore, the growth of transverse energy $\hbar\omega_\perp$ suppresses the transfer of kinetic energy of the soliton to transverse modes, resulting in the decay of the soliton [see Fig. 2(a)]. For a tight enough trapping potential ($\lambda = 30, \alpha = 1.93$) in Fig. 2(b), the instability does not occur as a consequence of the possibility of separation of the axial and transversal degrees of freedom. It is seen that the period of the stable soliton oscillation is $T_s = 1.7T_z$, which agrees well with that calculated by the BdG equations [14,15] for the case in the unitarity limit. As shown in the inset of Fig. 3, the soliton periods have a relatively weak dependence on the anisotropy, that is, larger values of λ yield smaller periods. Notice that under conditions of tight transverse confinement $\lambda = 30$ and small number pairs $N = 2 \times 10^2$, the system is in the quasi-1D regime, which corresponds to the cases discussed by the mean-field theory [14,15]. We also present the spatiotemporal evolutions of dark solitons in the quasi-1D regime for the cases of the BEC side in Fig. 2(c) and BEC limit in Fig. 2(d), respectively.

Figure 3 shows our results (□) on the periods T_s of dark soliton in the quasi-1D regime as a function of the dimensionless interaction parameter $\eta \equiv 1/k_F a_s$. The decrease of T_s as one moves from the BCS regime to the BEC limit is consistent with the mean-field theory computations by Scott *et al.* (△) [14] and Liao and Brand (▽) [15]. In the BEC limit ($\eta = 6$), our result is very close to the well-known value $\sqrt{2}T_z$ for atomic BECs [45–47], which is indicated by the horizontal dashed line in Fig. 3. We find that in the BEC regime ($\eta > 0$), our results are slightly larger than those based on the extended BdG equations. This is because the BdG equations cannot obtain the beyond-mean-field term of the equation of state correctly [9]. Notice that the order-parameter equation fails to give correct results on the BCS side. For comparison purposes, we also present our results on the BCS side ($\eta < 0$). Interestingly, different from the small discrepancy in the BEC regime, in the BCS side the BdG results are significantly larger than our results, which may be interpreted by the coupling to fermionic quasiparticle excitations near the soliton [14], which is completely disregarded in the order-parameter equation.

IV. SNAKE INSTABILITY OF UNITARY FERMI GASES

Dark solitons have 1D character and are stable in the quasi-1D regime, but they feature a long-wavelength transverse instability known as the "snake instability" [54–58] when extended into higher dimensions. The snake instability originates from the transfer of the soliton kinetic energy to the transverse modes parallel to the soliton nodal plane. Generally, dark solitons undergo a snake deformation, causing the nodal plane to collapse into vortex rings [56–58] in 3D (or vortex-antivortex pairs in two dimensions [55]). For atomic BECs, it has been shown that this instability leads to a strong bending of the nodal plane, which breaks down into vortex rings and sound waves, as experimentally observed [59,60].

The snake stability of dark solitons of superfluid Fermi gases in the unitarity limit can be studied by monitoring the evolution of a standing dark soliton created at the trap center [54–58]. The development of the snake instability and the concomitant vortex rings for a wide range of numbers of atom pairs with $\lambda = 6.5$ are displayed in Fig. 4(a) for $N = 2 \times 10^2$, Fig. 4(b) for 2×10^3, and Fig. 4(c) for 2×10^5, respectively. Vortex rings resemble toroids where the superfluid density is depleted, and so the slice of the vortex ring appears as two dark spots separated vertically. Since the presented density profile is symmetrical about the $x = 0$ axis, only the $x \geqslant 0$

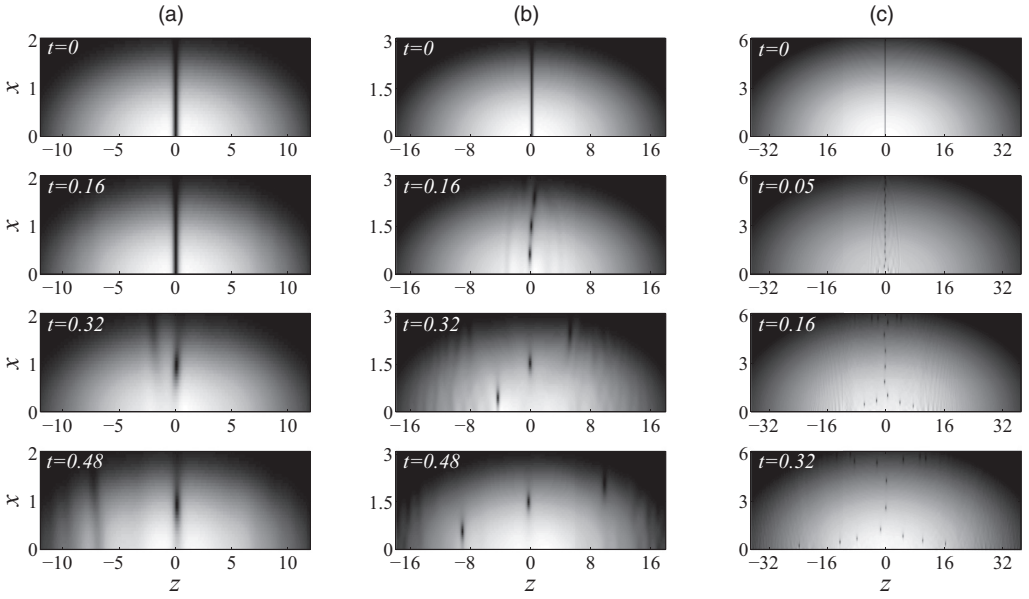

FIG. 4. Snapshots of the stationary dark-soliton dynamics in the unitarity limit with $\lambda = 6.5$. Planes (a), (b), and (c) correspond to the total numbers of atom pairs $N = 2 \times 10^2$, $N = 2 \times 10^3$, and $N = 2 \times 10^5$, respectively.

part is shown, where each vortex ring is indicated by one dark spot. As shown in Fig. 4(a), the stationary dark soliton is subject to the snake instability, bending into one vortex ring and sound waves, in strong contrast to the moving soliton slowly decaying into sound radiation (see Fig. 1). This is due to the larger dimensionality parameter $\alpha = \mu_G/\hbar\omega_\perp = 7.38$ at the trap center than that at the off-center position. As the number of atom pairs rises, the increased chemical potential opens more decay channels, which results in the formation of more vortex rings, that is, three ($\alpha = 15.90$) in Fig. 4(b) and 14 ($\alpha = 73.80$) in Fig. 4(c). From plane (a) to (c) the chemical potential increases tenfold and inversely, the size of solitons or vortex rings decreases threefold. We can estimate the size in the experimentally relevant case of $N = 2 \times 10^5$ in Fig. 4(c). The size scale is given by $\xi = R_z/959 = 0.29$ μm, which is too small to be resolved by optical means directly but by the time-of-flight expansion acting as a magnifying glass [11]. In addition, we find the time for the start of snake instability reduces significantly from $0.32T_z$ in Fig. 4(a) to $0.05T_z$ in Fig. 4(c).

Now we show how the instability mechanism can be suppressed under tight transverse confinements [61] and determine the criterion for stability against the transverse decay [51]. We consider the superfluid Fermi gases containing $N = 2 \times 10^4$ atom pairs in the unitarity limit and examine the evolution of dark solitons generated at an off-center position of $3R_z/4$. Figure 5 shows the density (left planes) and corresponding phase (right planes) of the evolutions of the solitons at the time when the solitons reach the trap center. Planes (a), (b), (c), (d), and (e) correspond to $\lambda = 6.5$, 50, 100, 180, and 250, respectively, and the evolution time $t = 0.56$, 0.53, 0.47, 0.45, and 0.42, respectively.

With a weak transverse trapping $\lambda = 6.5$ in Fig. 5(a), the created soliton subject to snake instability is decayed to vortex rings, one of which reaches the trap center at $0.56T_z$. Vortex rings can be evidenced by the 2π phase change at any point of the circle, as shown in the right plane of Fig. 5(a). Increasing the transverse frequency $\lambda = 50$ in Fig. 5(b) leads to a decrease in the bending of the soliton, and hence the production of a single vortex ring. It is seen only by observing dips in the density profile from the left plane of Fig. 5(b); it is very hard to discriminate between the soliton and the vortex rings. We find that the vortex ring evolves back into a soliton when moving near the ends of the trap due to the decrease of the dimensionality parameter. It is seen that such a periodic soliton or vortex ring is stable with an oscillation period of $2.2T_z$, which was observed first in atomic BECs [62]. In the

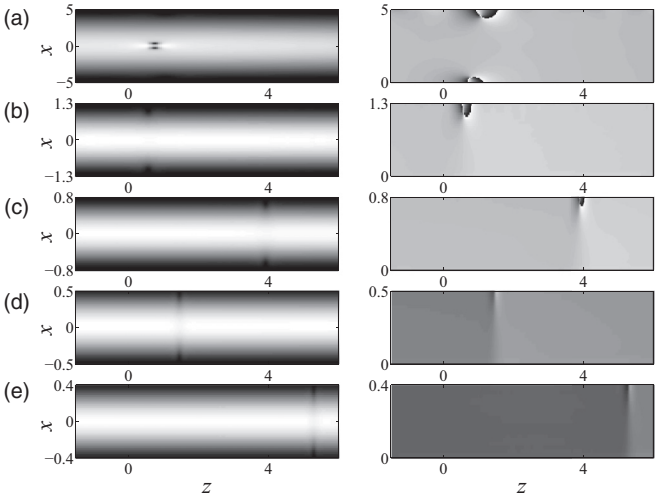

FIG. 5. Close-up snapshots of density (left) and phase (right) profiles of the evolutions of the off-centered dark solitons initially generated at $3R_z/4$, when they evolve near the center of the unitary Fermi gases with $N = 2 \times 10^4$ for different transverse confinements. Planes (a), (b), (c), (d), and (e) correspond to $\lambda = 6.5$, 50, 100, 180, and 250, and evolution time $t = 0.56$, 0.53, 0.47, 0.45, and 0.42, respectively.

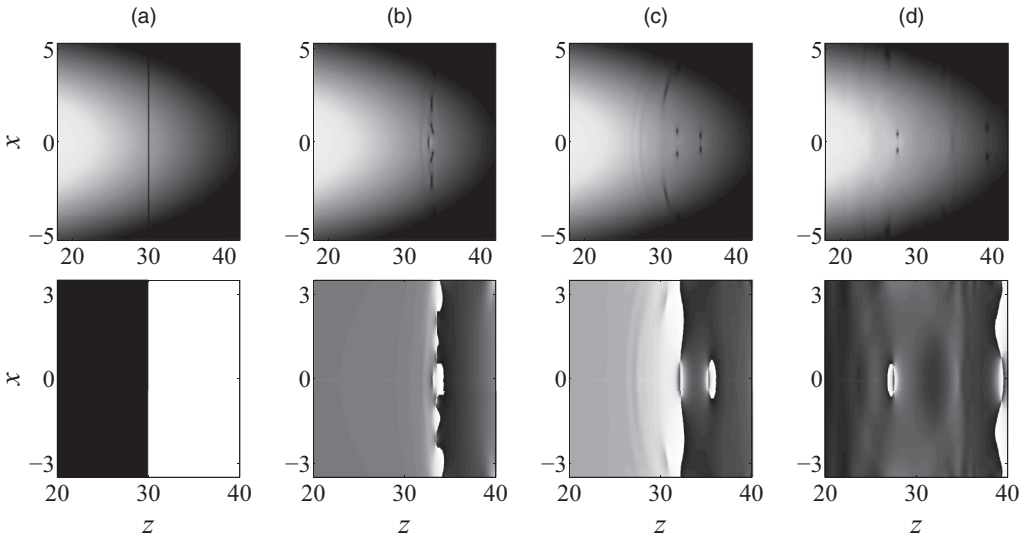

FIG. 6. Close-up snapshots of the evolution of density (top) and corresponding phase profiles (bottom) for the dark-soliton dynamics in the unitary Fermi gas with the MIT experimental parameters of $N = 2 \times 10^5$ and $\lambda = 6.5$ at (a) $t = 0$, (b) $t = 0.07$, (c) $t = 0.12$, and (d) $t = 0.24$, showing the onset of the snake instability and the decay of the soliton into two vortex rings, as evidenced by the corresponding phase profiles.

geometries $\lambda = 100$ in Fig. 5(c) and $\lambda = 180$ in Fig. 5(d), where the soliton is transversely unstable but the transverse width of the system is too small to support vortex rings, an excitation with soliton and vortex properties, known as a hybrid of soliton and vortex rings [62,63], is predicted to occur. The hybrid of solitons and vortex rings can be evidenced in the right planes by the emergence of not only phase azimuthal dependence but also a phase jump, which is characteristic of a soliton. We find that the oscillation period of the soliton and vortex ring hybrid is $2.0T_z$ for the case of Fig. 5(c). Finally, a very tight transverse confinement ($\lambda = 250$) results in a highly elongated quasi-1D geometry, evidenced by a stable soliton with its step phase profile shown in Fig. 5(e). The period of the stable soliton in such a highly elongated geometry is found to be $1.83T_z$, only 8% larger than that in the quasi-1D regime.

Therefore, the criterion of dynamical stability of dark solitons in trapped unitary Fermi gases can be estimated [51] by the case of Fig. 5(e), which is $\alpha_c = \mu_s/\hbar\omega_\perp = 4.2$. We find that the stability criterion (i.e., $\alpha < \alpha_c$) is very strict for the conditions of current experiments. A system with a total number of atom pairs of 10^5 in most Fermi experiments requires at least $\lambda = 1500$ in the unitarity limit when solitons are generated in the off-center position of $3R_z/4$, while only $\lambda = 350$ is required for $\alpha_c = 2.4$ of weakly interacting atomic BECs [54].

V. COMPARISON WITH EXPERIMENT

In the MIT experiment [11], the superfluid Fermi gas containing 2×10^5 atom pairs was prepared in a cylindrically symmetric trap with $\omega_z = 2\pi \times 10.66$ Hz and $\lambda = 6.5$. In order to observe dark-soliton dynamics in the Fermi gas, they optically applied a step-function potential to advance a π phase shift of the superfluid order parameter, thereby imprinting a moving soliton at the off-center position.

We perform numerical simulations using the experimental parameters in the unitary limit. The results of the close-up snapshots of density profiles (top row) of dark-soliton dynamics and corresponding phase profiles (bottom row) are presented in Fig. 6. In Fig. 6(a), the initial soliton has a node of zero density at $3R_z/4$ (top) and a π phase step (bottom). As the soliton starts to move at $t = 0.07$ (6.56 ms), the soliton plane is dynamically unstable and subject to a gradual bending, as shown in Fig. 6(b), resulting from the inhomogeneous transverse density. Subsequently, as shown in Fig. 6(c), the soliton plane tears into pieces, creating two vortex rings and radiating sound waves. The vortex rings are evidenced azimuthally by a 2π phase dependence in the bottom plane. At 11.2 ms [Fig. 6(c)], the two vortex rings produced propagate in opposing directions, that is, the inner ring initially propagates to the right and the outer to the left. Finally, the vortex ring propagating right is absorbed by the boundary and only the left vortex ring survives. Note that the dimensionality parameter at the $3R_z/4$ position is $\alpha = 32$, much larger than the stability criterion $\alpha_c = 4.2$ estimated by us, so such a decay channel can be anticipated.

It is interesting to investigate the evolution of the survival vortex ring in the trapped Fermi gas. As shown in Fig. 7, we find that the vortex ring is stable and presents an oscillation in a solitonlike manner, which is highlighted by red lines. Interestingly, after reflecting at the left end, it also disappears as it moves to the right boundary; thus only a single oscillation period can be observed. This period is given by about $2.8T_z$, which is nearly 2 times the soliton period of $1.7T_z$ and also differs from the period of $2.0T_z$ for a hybrid of solitons and vortex rings. The results suggest that in a strongly interacting superfluidity, to probe the 1D character of stable solitons one needs a very small number of atoms or very high trap anisotropy to guard against snake instability, which is difficult to achieve in the current experimental situation. However, this may be an ideal system to experimentally study the

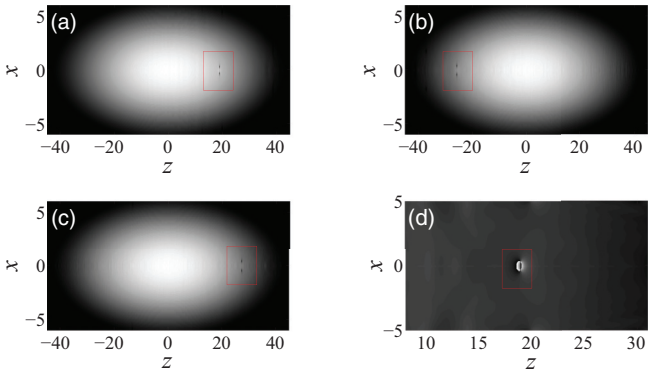

FIG. 7. (Color online) Snapshots of the oscillation of a vortex ring created by the snake instability of the unitary Fermi gases from Fig. 6 at (a) $t = 0.4$ as well as (d) the corresponding phase, (b) $t = 2.0$, and (c) $t = 2.8$.

dynamics of vortex rings or hybrids of solitons and vortex rings resulting from snake instability, which can be distinguished by measuring different oscillation periods or their phase profiles, as we discussed.

VI. CONCLUSIONS

We perform the calculations for the dynamics and stability of dark solitons in anisotropic superfluid Fermi gases for a wide range of atomic particle numbers and aspect rations within the framework of the order-parameter equation. We study the dynamics of solitons in the trapped superfluid Fermi gases with a small number of atoms, and the computed soliton period of $1.7T_z$ in the unitary limit is in good agreement with one by the BdG equations. The snake instability of unitary Fermi gases is studied. By examining the evolutions of an initially off-center dark soliton under various aspect ratios, and a transition from hybrids of solitons and vortex rings to a stable soliton discriminated by their phase profiles, we give the criterion for stability against transverse decay, which is $\alpha_c = 4.2$. In addition, it is found that the soliton period of $1.83T_z$ increases 8% as the number of atom pairs is increased 2 orders, and the hybrid of solitons and vortex rings has a larger period of $2.0T_z$. We simulate the recent MIT experiment on the dark-soliton dynamics in the unitary Fermi gas. Instead of performing a very slow oscillation, as observed experimentally, the imprinted soliton is found to evolve into vortex rings which propagate in solitonlike manner with a period of $2.8T_z$. Such disagreement between theory and experiment may be accounted for by the time-of-flight method with Feshbach resonance, which will be considered in the future.

Note added in proof. Recently, we noted Refs. [64] and [65] addressing similar problems.

ACKNOWLEDGMENTS

We gratefully acknowledge Renyuan Liao, Hui Zhai, and Chao Hang for enlightening discussions and helpful comments. W.W. is supported by the NSFC under Grant No. 11105039, Fundamental Research Funds for the Central Universities of China (Programs No. 2012B05714 and No. 2010B23414), and the Doctoral Foundation of Hohai University 2010. X.D.M. is supported by the NSFC under Grant No. 11264039, and the Key Research Project of Xinjiang Higher Education, China, under Grant No. XJED2010141.

[1] T. Dauxois and M. Peyrard, *Physics of Solitons* (Cambridge University Press, Cambridge, UK, 2006).
[2] C. J. Pethick and H. Smith, *Bose-Einstein Condensation in Dilute Gases*, 2nd ed. (Cambridge University Press, Cambridge, UK, 2008).
[3] *Emergent Nonlinear Phenomena in Bose-Einstein Condensates*, edited by P. G. Kevrekidis, D. J. Frantzeskakis, and R. Carretero-González (Springer-Verlag, Berlin, 2008).
[4] D. J. Frantzeskakis, J. Phys. A: Math. Theor. **43**, 213001 (2010).
[5] K. M. O'Hara, S. L. Hemmer, M. E. Gehm, S. R. Granade, and J. E. Thomas, Science **298**, 2179 (2002).
[6] C. A. Regal, M. Greiner, and D. S. Jin, Phys. Rev. Lett. **92**, 040403 (2004).
[7] M. Bartenstein, A. Altmeyer, S. Riedl, S. Jochim, C. Chin, J. H. Denschlag, and R. Grimm, Phys. Rev. Lett. **92**, 120401 (2004).
[8] M. W. Zwierlein, C. A. Stan, C. H. Schunck, S. M. F. Raupach, A. J. Kerman, and W. Ketterle, Phys. Rev. Lett. **92**, 120403 (2004).
[9] S. Giorgini, L. P. Pitaevskii, and S. Stringari, Rev. Mod. Phys. **80**, 1215 (2008), and references therein.
[10] A. Adams, L. D. Carr, T. Schäfer, P. Steinberg, and J. E. Thomas, New J. Phys. **14**, 115009 (2012).
[11] T. Yefsah, A. T. Sommer, M. J. H. Ku, L. W. Cheuk, W. Ji, W. S. Bakr, and M. W. Zwierlein, Nature (London) **499**, 426 (2013).
[12] M. Antezza, F. Dalfovo, L. P. Pitaevskii, and S. Stringari, Phys. Rev. A **76**, 043610 (2007).
[13] A. Spuntarelli, L. D. Carr, P. Pieri, and G. C. Strinati, New J. Phys. **13**, 035010 (2011).
[14] R. G. Scott, F. Dalfovo, L. P. Pitaevskii, and S. Stringari, Phys. Rev. Lett. **106**, 185301 (2011).
[15] R. Liao and J. Brand, Phys. Rev. A **83**, 041604(R) (2011).
[16] R. G. Scott, F. Dalfovo, L. P. Pitaevskii, S. Stringari, O. Fialko, R. Liao, and J. Brand, New. J. Phys. **14**, 023044 (2012).
[17] A. Bulgac, Y.-L. Luo, and K. J. Roche, Phys. Rev. Lett. **108**, 150401 (2012).
[18] W. Wen and G. X. Huang, Phys. Rev. A **79**, 023605 (2009).
[19] A. Khan and P. K. Panigrahi, J. Phys. B: At., Mol. Opt. Phys. **46**, 115302 (2013).
[20] P. G. de Gennes, *Superconductivity of Metals and Alloys* (Addison-Wesley, New York, 1989).
[21] L. Salasnich, N. Manini, and F. Toigo, Phys. Rev. A **77**, 043609 (2008); L. Salasnich and F. Toigo, *ibid.* **78**, 053626 (2008).
[22] W. Wen, Y. Zhou, and G. X. Huang, Phys. Rev. A **77**, 033623 (2008).
[23] Y. E. Kim and A. L. Zubarev, Phys. Rev. A **70**, 033612 (2004).
[24] A. L. Zubarev, J. Phys. B: At., Mol. Opt. Phys. **42**, 011001 (2009).

[25] S. K. Adhikari, Phys. Rev. A **77**, 045602 (2008).
[26] F. Ancilotto, L. Salasnich, and F. Toigo, Phys. Rev. A **85**, 063612 (2012).
[27] S. K. Adhikari, J. Phys. B: At., Mol. Opt. Phys. **43**, 085304 (2010).
[28] G. Rupak and T. Schäfer, Nucl. Phys. A **816**, 52 (2009).
[29] H. W. Xiong, S. J. Liu, and M. S. Zhan, Phys. Rev. A **74**, 033602 (2006).
[30] G. E. Astrakharchik, J. Boronat, J. Casulleras, and S. Giorgini, Phys. Rev. Lett. **93**, 200404 (2004).
[31] N. Manini and L. Salasnich, Phys. Rev. A **71**, 033625 (2005).
[32] G. Diana, N. Manini, and L. Salasnich, Phys. Rev. A **73**, 065601 (2006).
[33] W. Wen, S.-Q. Shen, and G. X. Huang, Phys. Rev. B **81**, 014528 (2010).
[34] P. Nozières and S. Schmitt-Rink, J. Low Temp. Phys. **59**, 195 (1985).
[35] P. Pieri and G. C. Strinati, Phys. Rev. Lett. **91**, 030401 (2003).
[36] M. M. Forbes and R. Sharma, arXiv:1308.4387.
[37] A. Bulgac, Y.-L. Luo, P. Magierski, K. J. Roche, and Y. Yu, Science **332**, 1288 (2011).
[38] L. Salasnich, F. Ancilotto, N. Manini, and F. Toigo, Laser Phys. **19**, 636 (2009).
[39] F. Ancilotto, L. Salasnich, and F. Toigo, Phys. Rev. A **79**, 033627 (2009).
[40] H. Zhai and T.-L. Ho, Phys. Rev. Lett. **97**, 180414 (2006).
[41] Ł. Dobrek, M. Gajda, M. Lewenstein, K. Sengstock, G. Birkl, and W. Ertmer, Phys. Rev. A **60**, R3381 (1999).
[42] S. Burger, K. Bongs, S. Dettmer, W. Ertmer, K. Sengstock, A. Sanpera, G. V. Shlyapnikov, and M. Lewenstein, Phys. Rev. Lett. **83**, 5198 (1999).
[43] J. Denschlag, J. E. Simsarian, D. L. Feder, C. W. Clark, L. A. Collins, J. Cubizolles, L. Deng, E. W. Hagley, K. Helmerson, W. P. Reinhardt, S. L. Rolston, B. I. Schneider, and W. D. Phillips, Science **287**, 97 (2000).
[44] P. Muruganandam and S. K. Adhikari, Comput. Phys. Commun. **180**, 1888 (2009).
[45] Th. Busch and J. R. Anglin, Phys. Rev. Lett. **84**, 2298 (2000).
[46] G. X. Huang, J. Szeftel, and S. H. Zhu, Phys. Rev. A **65**, 053605 (2002).
[47] V. A. Brazhnyi, V. V. Konotop, and L. P. Pitaevskii, Phys. Rev. A **73**, 053601 (2006).
[48] N. G. Parker, N. P. Proukakis, M. Leadbeater, and C. S. Adams, Phys. Rev. Lett. **90**, 220401 (2003); J. Phys. B: At., Mol. Opt. Phys. **36**, 2891 (2003).
[49] V. V. Konotop and L. Pitaevskii, Phys. Rev. Lett. **93**, 240403 (2004); V. A. Brazhnyi and V. V. Konotop, Phys. Rev. A **68**, 043613 (2003).
[50] D. E. Pelinovsky, D. J. Frantzeskakis, and P. G. Kevrekidis, Phys. Rev. E **72**, 016615 (2005).
[51] A. Muryshev, G. V. Shlyapnikov, W. Ertmer, K. Sengstock, and M. Lewenstein, Phys. Rev. Lett. **89**, 110401 (2002).
[52] G. Theocharis, P. G. Kevrekidis, M. K. Oberthaler, and D. J. Frantzeskakis, Phys. Rev. A **76**, 045601 (2007).
[53] A. Weller, J. P. Ronzheimer, C. Gross, J. Esteve, M. K. Oberthaler, D. J. Frantzeskakis, G. Theocharis, and P. G. Kevrekidis, Phys. Rev. Lett. **101**, 130401 (2008).
[54] A. E. Muryshev, H. B. van Linden van den Heuvell, and G. V. Shlayapnikov, Phys. Rev. A **60**, R2665 (1999).
[55] G. X. Huang, V. A. Makarov, and M. G. Velarde, Phys. Rev. A **67**, 023604 (2003).
[56] D. L. Feder, M. S. Pindzola, L. A. Collins, B. I. Schneider, and C. W. Clark, Phys. Rev. A **62**, 053606 (2000).
[57] J. Brand and W. P. Reinhardt, Phys. Rev. A **65**, 043612 (2002).
[58] P. G. Kevrekidis, G. Theocharis, D. J. Frantzeskakis, and A. Trombettoni, Phys. Rev. A **70**, 023602 (2004).
[59] Z. Dutton, M. Budde, C. Slowe, and L. V. Hau, Science **293**, 663 (2001).
[60] B. P. Anderson, P. C. Haljan, C. A. Regal, D. L. Feder, L. A. Collins, C. W. Clark, and E. A. Cornell, Phys. Rev. Lett. **86**, 2926 (2001).
[61] N. P. Proukakis, N. G. Parker, D. J. Frantzeskakis, and C. S. Adams, J. Opt. B: Quantum Semiclass. Opt. **6**, S380 (2004).
[62] S. Komineas and N. Papanicolaou, Phys. Rev. Lett. **89**, 070402 (2002); Phys. Rev. A **67**, 023615 (2003).
[63] I. Shomroni, E. Lahoud, S. Levy, and J. Steinhauer, Nat. Phys. **5**, 193 (2009).
[64] A. Bulgac, M. M. Forbes, M. M. Kelley, K. J. Roche, and G. Wlazłowski, arXiv:1306.4266.
[65] A. Cetoli, J. Brand, R. G. Scott, F. Dalfovo, and L. P. Pitaevskii, Phys. Rev. A **88**, 043639 (2013).